Proceedings of the 6th International Conference on the Application of Physical Modelling in Coastal and Port Engineering and Science (Coastlab16)

Ottawa, Canada, May 10-13, 2016

OPTICAL TRACKING OF WATER-BORNE DEBRIS IN LABORATORY CONDITIONS

JACOB STOLLE[1], IOAN NISTOR[1], AND NILS GOSEBERG[1,2]

1 University of Ottawa, Canada, jstol065@uottawa.ca, inistor@uottawa.ca

2 Institute for Hydraulic, Estuarine and Coastal Engineering, Leibniz University of Hannover, goseberg@fi.uni-hannover.de

ABSTRACT

The paper outlines a camera-based object tracking algorithm to track water-borne debris in high-velocity flow. The algorithm uses image processing techniques to identify the debris within the image and assigns unique identifiers to each debris to track the debris through an area of interest (AOI). The algorithm uses color thresholding and blob analysis to identify the debris within the image. A Kalman Filter is used to predict the trajectory of the debris and the Munkres algorithm is used to assign the predicted position of the debris to the observed position of the debris in the image. The accuracy of the algorithm is validated by tests performed with scaled-down shipping containers in the new Tsunami Wave Basin (TWB) at Waseda University. The algorithm performs well when compared to a manual image-by-image tracking method, however due to poor lighting conditions of the outdoor TWB small errors occur. The algorithm has many applications in the Coastal Engineering field from tracking the scour around a structure to the movement of armor units in a breakwater.

KEYWORDS: Debris, Camera-based Tracking, Physical Modeling, Tsunamis, Coastal Engineering

1 INTRODUCTION

Large-scale hydraulic events, such as floods, storm surges, and tsunamis, have become increasingly catastrophic as world-wide intensification of coastlines and sea level rise place a larger portion of the global population vulnerable. As a result, research and governing bodies have been focusing on evaluating the capacity of local at-risk communities to deal with the extreme forces associated with these large-scale events. For tsunamis in particular, recent efforts have led to new guidelines (FEMA P646, 2008) and standards (ASCE 7: Tsunami Loads and Effects, due 2016) to assist communities in the design and preparation for these events. In determining the design loads for critical structures, the focus has largely been on the hydraulic loads on structures (Ramsden, 1996; Arnason et al., 2009; Nouri et al., 2010; St-Germain et al., 2013), debris loads on structures (Haehnel and Daly, 2004; Matsutomi, 2009; Riggs et al., 2014; Aghl et al., 2015) and inundation limits (Titov and Synolakis, 1998; Mori et al., 2011; Goseberg, 2013). Whereas areas vulnerable to hydraulic loads has been evaluated by extensive analysis of inundation limits, areas at risk of debris loads has been difficult to determine.

The difficulty in determining areas vulnerable to debris impact span the three primary research methods in tsunami engineering: field surveys, numerical modeling, and physical modeling. In field surveys of devastated communities, determining the source of debris after the event (and therefore its motion throughout the event) can be difficult as many types of debris, such as vehicles, hydro poles, and shipping containers, are common to the local community (Naito et al., 2014). In numerical modeling, the coupling of solid-liquid numerical solver can be computationally expensive and a lack of a high-quality benchmarks for the models make obtaining useful results difficult (Canelas et al., 2013; Wu et al., 2014). In physical modeling, the random nature of debris motion makes obtaining statistically meaningful results time-consuming as numerous experiments and large quantities of data are needed (Matsutomi, 2009). Therefore, developing a method of quickly and accurately tracking and quantifying debris motion is necessary to help in both physical modeling and the development of benchmarks for numerical modeling.

Historically, the evaluation of debris motion was accomplished by determining the maximum shore-perpendicular displacement of the debris (Imamura et al., 2008), important in determining vulnerable areas but does not properly capture the intermediate variables, such as velocity, acceleration, and orientation, important in determining impact loads. The other option was a manual image-by-image analysis (Matsutomi et al., 2008; MacVicar and Piégay, 2012), which allowed for the capture of the intermediate variables but was extremely time-consuming. More recently, optical tracking methods have made the quantification of debris motion simpler and less time-consuming. Rueben et al. (2014) used a binary optical tracking

method. It successfully identified the top of the box based on a particular color and determined the box identification based on a pattern on the top. The method allows for the quick and accurate tracking of multiple boxes. However due to the requirement of the method to discern the pattern on the top of the box, the boxes had to be large enough to identify the pattern or a camera with sufficient resolution (which can be expensive), which can be limiting in some lab environments. Ali and Tougne (2009) used a spectral analysis of images to determine the presence of woody debris in a river. The method could handle the varying light conditions of the outdoor environment, though the method could not continue tracking the debris if the debris was temporarily occluded.

This paper presents a novel camera-based optical tracking algorithm to quickly and accurately track the motion of water-borne debris. The algorithm is implemented using MATLAB and many of the components of the algorithm are available open-source. The algorithm was evaluated using tests presented in Stolle et al. (2015) and Nistor et al. (2016) at Waseda University, and aims to:

- Consistently and automatically detect debris through the area of interest (AOI).
- Accurately track the centroids of the debris through the AOI.
- Maintain accurate and consistent tracking despite varying lighting conditions.

The paper is organized as follows: "Experimental Setup" outlines the setup of the experiment used to evaluate the algorithm; "Manual Tracking" outlines the image-by-image tracking used to evaluate the accuracy of the algorithm; "Optical Tracking Algorithm" outlines the parts of the algorithm and the steps involved in the automatic tracking of the debris; "Results" show the comparison between the algorithm and the manual tracking method; "Discussion" outlines the strengths and weaknesses of the algorithm; and "Conclusions and Outlook" summarizes the paper and discusses recommendations for future work.

2 EXPERIMENTAL SETUP

The experiments were conducted in the Coastal Engineering and Management Laboratory at the Department of Civil and Environmental Engineering at Waseda University, Tokyo, Japan. For these tests, an innovative, newly-constructed Tsunami Wave Basin (TWB) of 4-by-9 m dimension was utilized (**Error! Reference source not found.**). The TWB was equipped with a four-chamber overhead reservoir, fillable with a vacuum pump (TST-150, Sato Vac Inc., Japan). The maximum achievable hydraulic head with reference to still water elevation was 0.77 m. The water impoundment was released through computer-controlled air valves (SVB1V-50F-02HS, CKD Corporation, Japan).

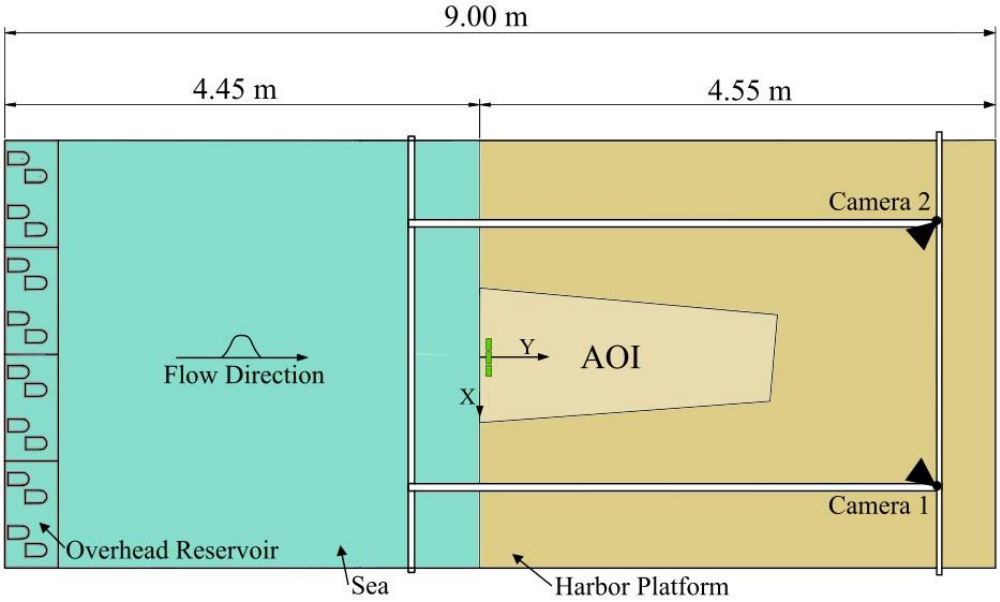

Figure 1. Plan View of the Experimental Setup of the Tsunami Wave Basin (TWB) at Waseda University, Tokyo, Japan.

At the opposite end of the wave basin an elevated, rigid horizontal apron, mimicking a harbor platform, was constructed. A vertical quay wall separated the "sea" section of the basin from the horizontal apron. A right-handed coordinate system with the origin at the midpoint of the edge of the quay wall was used throughout the tests. The y-axis was positive in the onshore direction of the wave propagation. The vertical axis was positive opposite to the gravity vector with z = 0 at the elevation of the apron area.

The water released from the overhead reservoir would propagate through the "sea" section as an elongated solitary

wave. When the wave reached the vertical quay wall, the wave would break and propagate over the harbor platform as a bore. For further analysis of the hydrodynamic condition see Nistor et al. (2016).

Two high-definition (HD) cameras (Basler AG, pi1900-32gc, Germany) were mounted at the apron end of the wave basin on an instrument frame at a height of 2.95 m above the apron area and pointing towards the quay wall edge. The debris consisted of an idealized 20-feet shipping containers (ISO668/688) down-scaled based on Froude similitude at a length scale of 1 in 40. The down-scaled shipping container, shown in Figure 2, were manufactured from positively buoyant polyethylene (PE-HMW, 0.92 g/cm³). The scaled shipping container had overall dimensions of 0.06 x 0.06 x 0.15 m with an approximate draft of 0.025 m. The debris was placed centered on the TWB harbor platform, 0.20 m in the positive y-direction from the vertical quay wall (Figure 1).

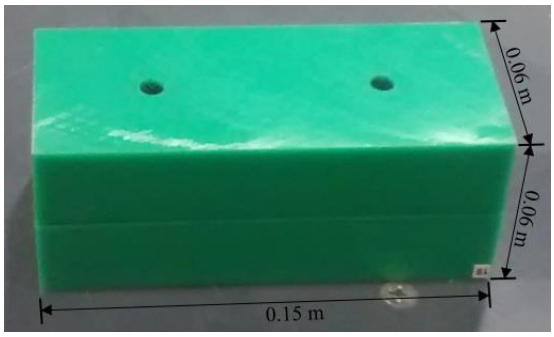

Figure 2. Idealized Shipping Container Model used as Debris (Scaled-down 20-feet shipping container).

3 MANUAL TRACKING

For validation purposes, a comparison between manually analyzed camera images and the algorithm was conducted to assess the general suitability of the algorithm. The two-dimensional (2D) trajectories obtained with the image processing algorithm were compared with positional information gathered from the manual method. The camera images were read in automatically by MATLAB. The four corners of the top of the container were selected to determine their pixel coordinates. The stored image coordinates were then transformed from pixel space into the real-world SI-unit space referenced by control points at the extrema of the AOI depicted in Figure 1. An estimated accuracy of ±10 pixel was obtained during the manual selection of the debris corners in the images due to some image blur related to the maximum available shutter speed of the cameras. Pixel to real-world coordinate ratios varied based on the non-orthographic angular field provided by the cameras. Values ranging from 6.41 – 10.74 pixel/cm in the (x)-direction and 5.59 – 5.92 pixel/cm in the (y)-direction were obtained. Thus, the SI-unit based accuracy of the manual image processing was determined to be in the range of 0.01 – 0.02 m in (x)-direction and 0.02 m in the (y)-direction. However, this does not allow to infer, that the optical system provides true reference values; thus, all comparisons between either recordings should rather be interpreted qualitatively at this stage.

4 OPTICAL TRACKING ALGORITHM

The optical tracking algorithm was developed, using image processing techniques, to detect and track the 2D trajectories of the water-borne debris. The algorithm was separated into three distinct parts: *Image Rectification*, *Object Detection*, and *Object Tracking*. *Image Rectification* is the process of preparing the image to be used within the algorithm. Within this part, corrections to the image due to lens distortion were made, the color space was adjusted, and the image was geo-referenced to determine real-world coordinates of the debris. *Object Detection* used the rectified image to determine the location of the debris within the image and determined the observed position of the debris. *Object Tracking* used the observed positions of the debris and assigned a unique identifier to each debris. The unique identifier allowed the debris to continually be tracked through the AOI. The following sections will go through these parts in more detail and discuss the methods involved.

4.1 IMAGE RECTIFICATION

Image Rectification is the process of preparing the image for use within the algorithm. The algorithm initially received a raw image from the camera (Figure 3(a)). Commonly, raw images may exhibit lens distortion due to the use of lower quality lenses (Wu and Kofman, 2004). Lens distortion was evaluated by determining if straight lines in the scene are also straight within the image plane. Based on this approach, it was found HD cameras had little to no distortion, therefore no lens correction was needed.

One of the objectives of this algorithm was to be able to accurately track the debris within variable lighting. This was needed as the TWB was located outdoors therefore there was a shift in lighting as the day progressed resulting in vastly different lighting conditions between the different experiments. The method used to address this issue was to change the color

space of the image. The color space is a three-dimensional geometric space with axis that can appropriately define all possible color perceptible to humans (Kuehni, 2003). The color space was particularly critical to the algorithm presented here as the *Object Detection* used color thresholding (section 4.2) to detect the debris. The raw color image expressed each pixel within the Red-Green-Blue (RGB) color space, however the RGB color space has redundancies associated with the expression of individual colors (Chai and Bouzerdoum, 2000). The redundancies resulted in difficulties in color thresholding, particularly with the variable lighting, as larger thresholds were needed to detect the debris, resulting in a noisy thresholded image. These redundancies were also an issue historically when image compression was needed, therefore a new family of color spaces was developed to separate the RGB color space into luminance and chrominance (Sharma and Bala, 2002). Particularly, for the algorithm used throughout this paper the Luminance-Blue-Difference Chroma-Red-Difference Chroma (YC_bC_r) color space proved advantageous.

As can be seen in Figure 3(b) and (c), the YC_bC_r color space has a smaller range of pixel values, particularly for the chromas. The chromas were the values that allow the algorithm to track a particular color (in this case the color 'green'), while the luminance determined the shading. The smaller range of values resulted in a smaller thresholding range, which reduced the noise in the color thresholded image.

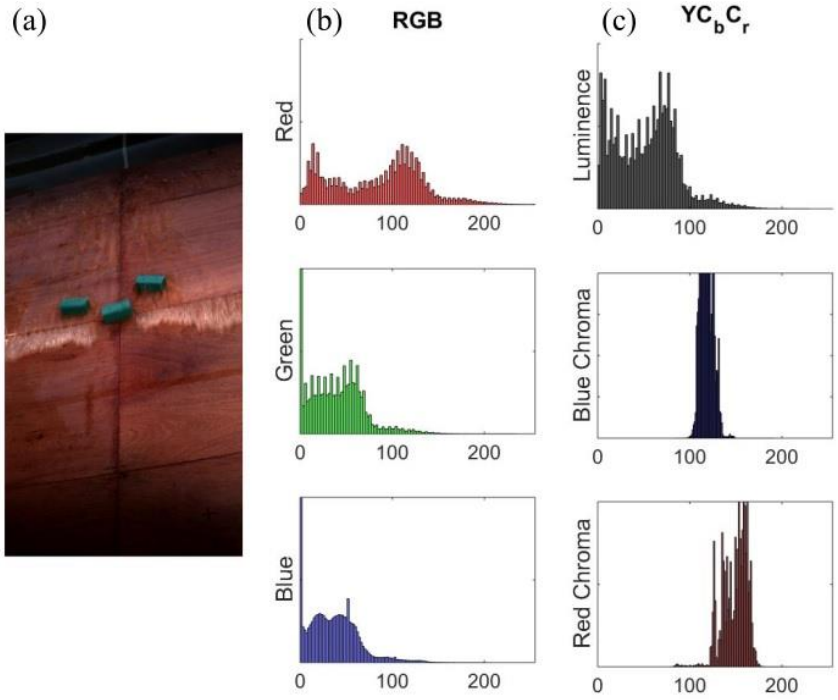

Figure 3. Color Space Adjustment for Experiment 11. (a) shows the image; (b) shows the RGB histogram (showing pixel count); and (c) shows the YC_bC_r histogram (showing pixel count).

The final process step of the *Image Rectification* was transforming the raw image from pixel coordinates to real-world coordinates (geo-rectification). The raw image pixels were labeled sequentially from the top left corner of the image (0,0) to the bottom right corner of the image (1928,1084). The pixel coordinates were transformed into real-world coordinates using three or more known control points (Holland and Holman, 1997) on the outside edges of the AOI. Each pixel was transformed by three separate adjustments: scaling, rotation, and translation. Using the pixel and real-world coordinates of the control points, the following system of linear equations was solved to determine the adjustment factors for the image:

$$\begin{bmatrix} x_f \\ y_f \\ 1 \end{bmatrix} = \begin{bmatrix} 1 & 0 & x_0 \\ 0 & 1 & y_0 \\ 0 & 0 & 1 \end{bmatrix} \begin{bmatrix} s & 0 & 0 \\ 0 & s & 0 \\ 0 & 0 & 1 \end{bmatrix} \begin{bmatrix} cos\theta & -sin\theta & 0 \\ sin\theta & cos\theta & 0 \\ 0 & 0 & 1 \end{bmatrix} \begin{bmatrix} x_i \\ y_i \\ 1 \end{bmatrix} \quad (1)$$

Where x_f is the real-world x-coordinate, y_f is the real-world y-coordinate, x_0 is the translation in the x-direction, y_0 is the translation in the y-direction, s is the scale factor, θ is the rotation factor, x_i is the pixel x-coordinate, y_i is the pixel y-coordinate. The resultant image of the geo-rectification can be seen in Figure 4a. Due to the experimental setup, the image plane was rectified on the horizontal bottom. This results in a small absolute error due to the difference between the top of the debris and the horizontal bottom, however all the error was compared relative to the manual tracking method which used the same rectification technique.

4.2 OBJECT DETECTION

Object Detection is the process of determining where the debris is within the image. Within image processing, this was done using image segmentation where an image is described by decomposing it into meaningful or spatially coherent regions sharing similar attributes (Harrabi and Braiek, 2012). In particular, this algorithm used one of the conventional image segmentation techniques, color thresholding. Applying it to a color image requires three thresholds (one for each axes of the color space). Determination of the threshold can be performed automatically (Harrabi and Braiek, 2011) or be pre-determined. As the containers are a uniform color, the pre-determined thresholds were much easier to select in this case.

Color thresholding performs a Boolean operation on each pixel within the image (Figure 4). If the pixel falls within each of the three thresholds (denoted in Figure 4(b) by yellow vertical solid lines), the pixel was assigned a "1" value. If the pixel falls outside of any of the thresholds, the pixel was assigned a "0" value. The resultant binary image is shown in Figure 4c, where the white pixels are the "1" values and the black pixels are the "0" values.

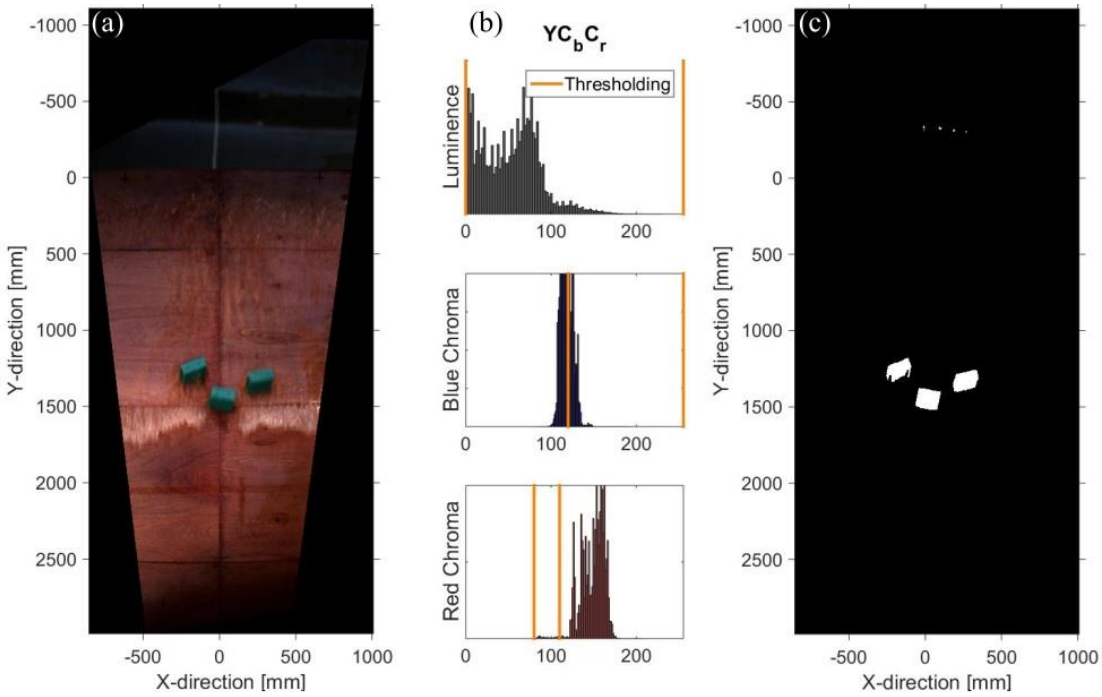

Figure 4. Color Thresholding. (a) shows the geo-rectified image; (b) shows the YC_bC_r histogram with thresholding limits; and (c) shows binary image after the color thresholding.

The segments of interest (in this case the debris) were determined within the image. The debris is of uniform shape therefore the relative shape of the debris is reasonably constant. However due to variation in lighting and the rotation of the debris, the size of the debris would change depending on the number of sides of the debris visible in the image. Using a technique called blob analysis, the algorithm searched the image for interconnected series of "1" pixels ("blob") and labels each "blob" with an integer value. The "blobs" found from the blob analysis were not necessarily the debris as stray pixel groups often fall within the color thresholds (e.g. around (0,-0.5) m in Figure 4(c)). To eliminate the noise, thresholding is again performed on the "blobs" to eliminate blobs smaller than a chosen value. This outlines the importance of a small thresholding range, if a larger range was necessary the "noise" blobs would be larger. The larger "noise" blobs would make thresholding out the "noise" blobs significantly more difficult. The "blobs" remaining after thresholding were considered to be the observed position of the debris.

4.3 OBJECT TRACKING

Object Tracking is the process of assigning a unique identifier (an integer) to each of the debris and maintaining the unique identifier on the debris throughout the AOI. Using *Object Detection*, a series of observed positions of the debris were determined, however the particular debris in the observed position was not known. *Object Tracking* assigned a unique identifier to the debris in the initial image and, using a Kalman Filter (Chan et al., 1979)and the Munkres algorithm (Munkres, 1957), assigned the unique identifier to the correct debris in the subsequent images.

Figure 5 outlines the method in which the algorithm maintained the unique identifiers. The algorithm relied on two functions to maintain the identifiers: Kalman Filter and Munkres algorithm (Munkres, 1957). When the identifier was initiated on a debris, a Kalman Filter was also created for each debris. The state equations for the Kalman Filter were derived using

simple 2D kinematics equations for displacement and velocity. Using the Kalman Filter and based on the previous observed positions of the debris, the trajectory of the debris could be estimated (Li et al., 2014). Figure 5 shows the predicted position of the debris in the current frame (star), based on the observed position in the previous frame (solid circle).

The predicted positions of the debris were then matched with observed positions of the debris in the current frame using an optimized matching algorithm, the Munkres algorithm (Munkres, 1957). The Munkres algorithm was used to minimize the cost of assignment between two sets of data (El-Anwar and Chen, 2012). In this case, the sets were the predicted and observed positions of the debris and the cost was the distance between the positions. A cost of no assignment was also used, which

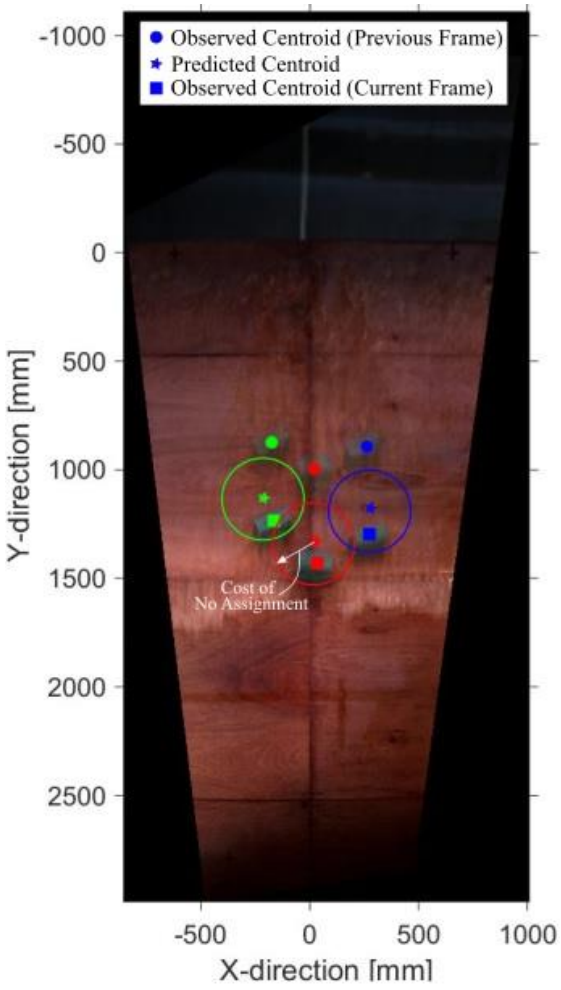

Figure 5. *Object Tracking*; combination of Kalman Filter and Munkres algorithm to maintain unique identifiers.

limited how far a predicted and observed position could be apart before no assignment would occur. The combination of the Munkres algorithm and the cost of no assignment created a search area (open circle) in the image for where the observed position should be (outlined in Figure 5). When the matching had been optimized, the unique identifiers were assigned to the observed position and the observed position was used to update the 2D trajectory in the Kalman Filter.

5 RESULTS

The camera-based optical tracking algorithm was validated using experiments performed at Waseda University, Tokyo, Japan. The results of the algorithm were compared to the manual tracking method, outlined in section 3 and quantified by an error metric. The error of the algorithm was determined as the 2D Euclidean distance between the manual tracking and algorithm position:

$$Error(t) = \sqrt{\left(x_{alg} - x_{man}\right)^2 + \left(y_{alg} - y_{man}\right)^2} \quad (2)$$

Where x_{alg} is the x-coordinate from the algorithm, x_{man} is the x-coordinate from the manual method, y_{alg} is the y-

coordinate from the algorithm, and y_{man} is the y-coordinate from the manual method.

Figure 6 shows the comparison of the algorithm and the manual tracking method for three experiments performed with one debris (Experiments #1, #5, and #7). The experiments were selected to evaluate the robustness of the algorithm due to their wide range of lighting condition. The debris was tracked through during the time in which the debris was travelling through the AOI. Due to variations in the velocity of the debris and since grounding occurred (Experiment #7), this results in differences in the length of time the debris was tracked for. Figure 6(a) shows the error between the algorithm and the manual tracking through time. As both techniques were evaluated on the same image set, the position in each image could be compared to the position in the manual tracking method. The algorithm performed well through the majority of the AOI with an average error of 0.025 m. The error between the algorithm and manual tracking method always occurred due to slight differences in the definition of the position of the debris. The algorithm defined the position of the debris as the centroid of the "blob" determined in the *Object Detection*. Due to the color thresholding method used, the algorithm detected any sides of the debris visible to the camera, which varied as the debris rotates. The shifting of the debris tracked resulted in a shift in the centroid as the debris rotated. The manual tracking method always tracked the position of the debris as the centroid of the top of the debris, therefore the sides of the debris were not considered in the determination of the position.

The increase of the error for all experiment, observed around 5 s in Figure 6(b), was due to the lack of lighting at the edge of the AOI. Due to the TWB being outside and a lack of available artificial lighting, the end of the AOI did not have enough light to properly track the debris. The change of color space was sufficient to deal with small changes in the light conditions but sufficient light was still needed for the color thresholding technique to still be valid.

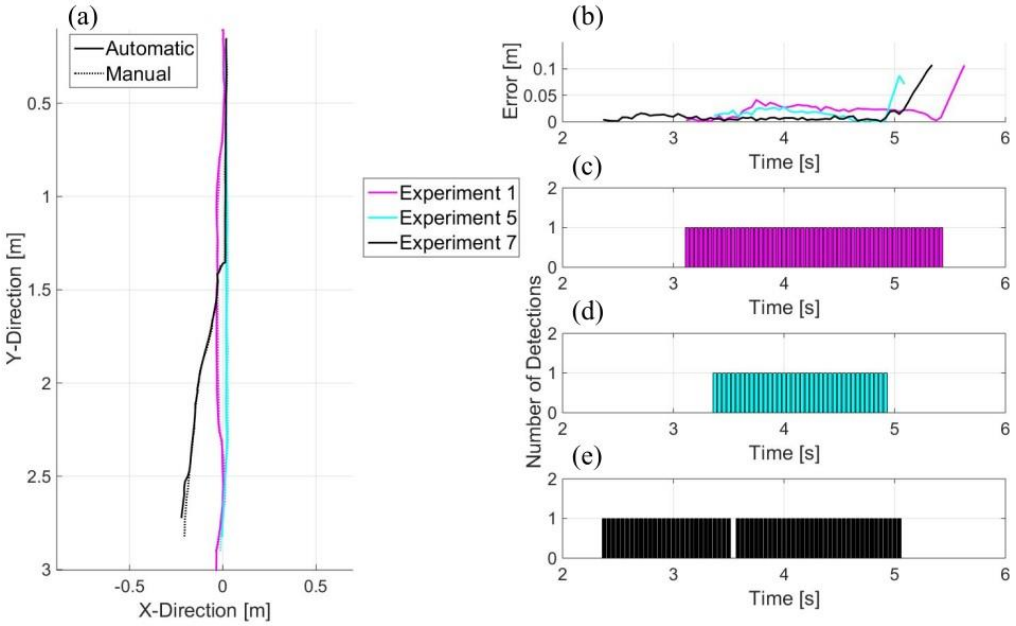

Figure 6. One Debris (Experiment #1, #5 and #7). (a) shows the comparison of the algorithm and manual results; (b) shows the error between the two methods; (c), (d), and (e) shows the number of detected debris in each image.

Figure 7 shows the comparison of the algorithm and the manual tracking method for three debris (Experiment #11). The algorithm performed similarly when compared with the experiments outlined in Figure 6 with a single debris involved. The average error for the experiment was 0.03 m. The slight increase in error can be attributed to two aspects of the experiment. As can be seen in Figure 5, near the vertical quay wall, where the debris are initially placed, there is a shaded section with a sharp edge between the shaded and lighted sections. As the debris cross this line, around 3 s, the "blob" in the *Object Detection* broke up due to the variance in lighting. This resulted in multiple smaller blobs, too small to be recognized as debris by the algorithm (Figure 7(c)). When the debris was occluded, like in this case, the algorithm considered the predicted positions of the debris (from the Kalman Filter) as the position of the debris. This process allowed the unique identifier to maintain the same trajectory as before the occlusion and when the debris was no longer occluded the unique identifier was again assigned to the correct observed position. While this process resulted in some error between the algorithm and manual tracking method, it was preferable to maintain the identifier instead of the debris being assigned a new identifier when the debris was observed again.

The second source of error with multiple debris occurred because the debris were moving with different velocities and trajectories, resulting in debris entering the section of the AOI with poor lighting at different instances. This can be observed

in particular with D2. Since the debris was within the AOI, the algorithm attempted to track the debris, however due to the poor lighting the algorithm was not detecting the debris. This resulted in the debris being occluded and the algorithm relied on the predicted position of the debris, which was increasingly out of date with each image the debris was not detected. The error from this case could similarly be avoided with better lighting at the edges of the AOI.

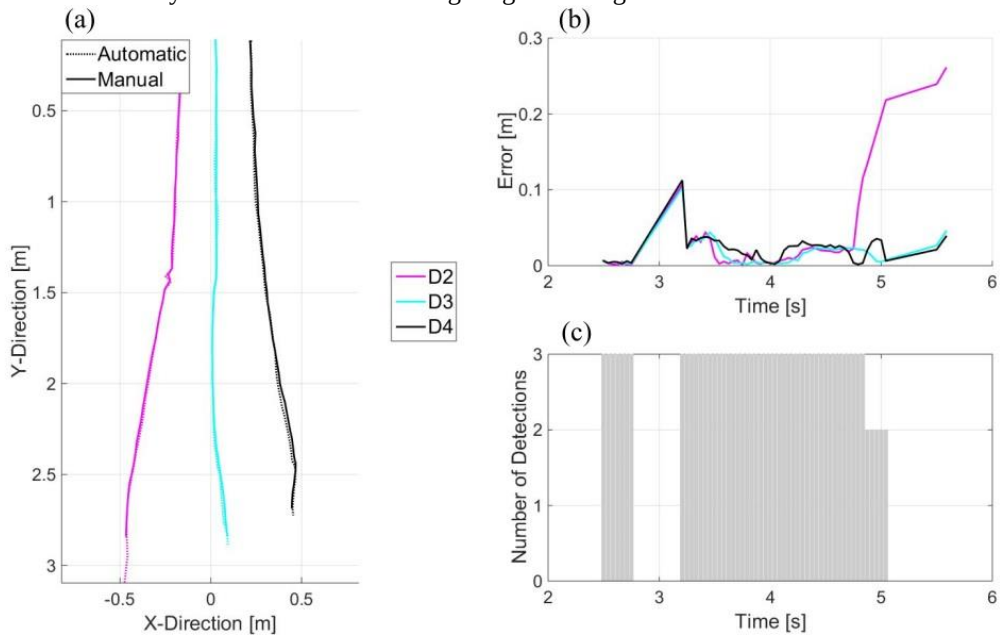

Figure 7. Three Debris (Experiment #11). (a) shows comparison of algorithm and manual tracking method; (b) shows the error between the two methods; and (c) shows the number of detected debris in each image.

6 DISCUSSION

The camera-based object tracking algorithm presented in the previous sections accurately tracked multiple debris through the AOI, outlined in Figure 1. The algorithm utilized image processing techniques to detect the debris within each image and consistently tracked the debris despite the varying lighting conditions. The algorithm used color thresholding to segment the image and determined the segments of the image that contained the debris. While the color thresholding performed well with the discrete debris experiment presented here, issues occur when the debris agglomerated. As the debris agglomerated, the color thresholding no longer distinguished between multiple debris. As the blob analysis was applied to the image, the algorithm determined multiple debris as one "blob" (and therefore one debris) since the pixels were interconnected. The discretization of these "blobs" with multiple objects of interest was a common issue within image processing. Multiple techniques have been suggested but further work is needed in evaluating these techniques (Ye et al., 2008; Omidvar et al., 2014).

The advantage of the color thresholding technique used for *Object Detection* was that the algorithm could be used at both larger and smaller scales. As long as the object of interest has a distinct color, compared to the rest of the image, the algorithm will be able to consistently and accurately track the object. This has a particular advantage on a smaller scale since methods like the one presented by Rueben et al. (2014) require a large enough object for the pattern to be clear and distinct in the image. The disadvantage occurred if the debris did not have a prevalent geometric feature. The debris in these test had an obvious long axis which allows the orientation of the debris to be tracked. If the debris did not have this feature, as in the cube in Rueben et al. (2014), the orientation will not be determined as the algorithm would have no basis to determine the orientation.

The algorithm used a Kalman Filter to predict the trajectory of the debris and allowed for more consistent assignment of the identifiers. The Kalman Filter also prevented identifiers from being lost when occlusion of the debris occurs. If occlusion of the debris occurred, the cost of no assignment prevented the assignment of the identifiers to a noise "blob". The algorithm received no assignment for the predicted position, and takes the predicted position as the position of the debris, continuing to the next frame. Once the debris was no longer occluded, the identifier was again assigned to the observed position. This process allowed the algorithm to continue to track the debris, and in the event of the wave overtopping the debris or an obstacle in the image, the algorithm could still be useful.

One of the primary issue of this particular validation experiments was due to the outdoor TWB. The outdoor setting resulted in varying light conditions, which made color thresholding difficult. The algorithm handled this issue by adjusting

the color space to reduce the redundancies associated with the RGB color space (Chai and Bouzerdoum, 2000). The algorithm handled the varying conditions relatively well. However, when there was very little light, like at the outside edges of the AOI, the algorithm did not detect the debris. The use of spectral analysis, as in Ali and Tougne (2009), could potentially improve the detection in these poorly lit areas.

7 CONCLUSIONS AND OUTLOOK

This paper introduced a camera-based optical tracking algorithm for tracking the motion of water-borne debris in high-velocity flows. The algorithm combined multiple techniques common to image processing, such as color thresholding, blob analysis, Kalman Filter, and the Munkres algorithm, to consistently track uniform debris through a specified AOI. To evaluate the applicability of the algorithm, a study was performed at Waseda University, Tokyo, Japan to track uniform shipping containers in high-velocity flow and the method was compared to manual tracking results to determine the accuracy of the method. The study showed that the algorithm could:

- Consistently detect the uniform debris through the AOI.
- Maintain consistent identifiers on the debris through the AOI.
- Remarkably accurate track the centroids of the debris through the AOI.
- Maintain accurate and consistent tracking despite varying lighting conditions.

While the algorithm performed well in the cases discussed here, significant work is needed to make the algorithm more robust in cases with more debris. Particularly in the cases where debris agglomeration occurred, the algorithm had difficulties determining the number of debris within the agglomeration and identifiers were not assigned to the correct debris. Despite these shortcomings, the algorithm has potential to be used in a wide variety of applications in the physical modeling of coastal processes. Similar techniques can be used to determine the time-history of scour around a structure, the movement of armor units in a breakwater, and the motion of granular material over a bed.

ACKNOWLEDGEMENT

The authors gratefully acknowledge the access to the new Tsunami Wave Basin provided by colleagues at Waseda University in Tokyo, Japan. N. Goseberg acknowledges that this research was supported by a Marie Curie International Outgoing Fellowship within the 7th European Community Framework Program. I. Nistor acknowledges that this research was supported by the Kajima Foundation, Japan and a NSERC Discovery Grant.

REFERENCES

Aghl, P.P., Naito, C., Riggs, H., 2015. Estimation of demands resulting from inelastic axial impact of steel debris. Engineering Structures 82, 11–21.

Ali, I., Tougne, L., 2009. Unsupervised video analysis for counting of wood in river during floods, in: Advances Visual Computing. Springer, pp. 578–587.

Arnason, H., Petroff, C., Yeh, H., 2009. Tsunami bore impingement onto a vertical column. Journal of Disaster Research 4, 391–403.

Canelas, R., Ferreira, R.M., Crespo, A., Domınguez, J., 2013. A generalized SPH-DEM discretization for the modelling of complex multiphasic free surface flows, in: 8thinternationalSPHERICworkshop.

Chai, D., Bouzerdoum, A., 2000. A Bayesian approach to skin color classification in YCbCr color space, in: TENCON2000.Proceedings. IEEE, pp. 421–424.

Chan, Y.T., Hu, A.G.C., Plant, J.B., 1979. A Kalman Filter Based Tracking Scheme with Input Estimation. Aerospace and Electronic Systems, IEEE Transactions on AES-15, 237–244.

El-Anwar, O., Chen, L., 2012. Maximizing the computational efficiency of temporary housing decision support following disasters. Journal of Computing in Civil Engineering 28, 113–123.

Goseberg, N., 2013. Reduction of maximum tsunami run-up due to the interaction with beachfront development - application of single sinusoidal waves. Nat Hazards Earth Syst Sci Disc 1, 1119–1171.

Haehnel, R.B., Daly, S.F., 2004. Maximum impact force of woody debris on floodplain structures. Journal of Hydraulic Engineering 130, 112–120.

Harrabi, R., Braiek, E., 2011. Color image segmentation using automatic thresholding techniques, in: Systems,Signals Devices (SSD), 2011 8th International Multi-Conference. IEEE, pp. 1–6.

Harrabi, R., Braiek, E.B., 2012. Color image segmentation using multi-level thresholding approach and data fusion techniques: application in the breast cancer cells images. EURASIP Journal on Image and Video Processing 2012, 1–11.

Holland, K.T., Holman, R.A., 1997. Video estimation of foreshore topography using trinocular stereo. Journal of Coastal Research 81–87.

Imamura, F., Goto, K., Ohkubo, S., 2008. A numerical model for the transport of a boulder by tsunami. Journal of Geophysical Research: Oceans (1978–2012) 113.

Kuehni, R.G., 2003. Color space and its divisions: color order from antiquity to the present. John Wiley & Sons.

Li, H., Bai, P., Song, H., 2014. Car tracking algorithm based on Kalman filter and compressive tracking, in: Image Signal Processing (CISP),

2014 7th International Congress. IEEE, pp. 27–31.

MacVicar, B., Piégay, H., 2012. Implementation and validation of video monitoring for wood budgeting in a wandering piedmont river, the Ain River (France). Earth Surface Processes and Landforms 37, 1272–1289.

Matsutomi, H., 2009. Method for estimating collision force of driftwood accompanying tsunami inundation flow. Journal of Disaster Research 4, 435–440.

Matsutomi, H., Fujii, M., Yamaguchi, T., 2008. Experiments and development of a model on the inundated flow with floating bodies. Coastal Engineering 1458–1470.

Mori, N., Takahashi, T., Yasuda, T., Yanagisawa, H., 2011. Survey of 2011 Tohoku earthquake tsunami inundation and run-up. Geophysical Research Letters 38.

Munkres, J., 1957. Algorithms for the assignment and transportation problems. Journal of the Society for Industrial & Applied Mathematics 5, 32–38.

Naito, C., Cercone, C., Riggs, H.R., Cox, D., 2014. Procedure for site assessment of the potential for tsunami debris impact. Journal of Waterway, Port, Coastal and Ocean Engineering 140, 223–232.

Nistor, I., Goseberg, N., Mikami, T., Shibayama, T., Stolle, J., Nakamura, R., Matsuba, S., 2016. Hydraulic Experiments on Debris Dynamics over a Horizontal Plane. In Review (Journal of Waterway, Port, Coastal, and Ocean Engineering).

Nouri, Y., Nistor, I., Palermo, D., Cornett, A., 2010. Experimental investigation of tsunami impact on free standing structures. Coastal Engineering Journal 52, 43–70.

Omidvar, M., Chen, Z., Iskander, M., 2014. Image-Based Lagrangian Analysis of Granular Kinematics. Journal of Computing in Civil Engineering 04014101.

Ramsden, J.D., 1996. Forces on a vertical wall due to long waves, bores, and dry-bed surges. Journal of waterway, port, coastal, and ocean engineering 122, 134–141.

Riggs, H., Cox, D., Naito, C., Kobayashi, M., Aghl, P.P., Ko, H.-S., Khowitar, E., 2014. Experimental and Analytical Study of Water-Driven Debris Impact Forces on Structures. Journal of Offshore Mechanics and Arctic Engineering 136, 041603.

Rueben, M., Cox, D., Holman, R., Shin, S., Stanley, J., 2014. Optical Measurements of Tsunami Inundation and Debris Movement in a Large-Scale Wave Basin. Journal of Waterway, Port, Coastal, and Ocean Engineering 141.

Sharma, G., Bala, R., 2002. Digital color imaging handbook. CRC press.

St-Germain, P., Nistor, I., Townsend, R., Shibayama, T., 2013. Smoothed-particle hydrodynamics numerical modeling of structures impacted by tsunami bores. Journal of Waterway, Port, Coastal, and Ocean Engineering.

Stolle, J., Nistor, I., Goseberg, N., 2015. Optical Tracking of Floating Shipping Containers in High-Velocity Flow. In Review (Coastal Engineering Journal).

Titov, V.V., Synolakis, C.E., 1998. Numerical modeling of tidal wave runup. Journal of Waterway, Port, Coastal, and Ocean Engineering.

Wu, T.-R., Chu, C.-R., Huang, C.-J., Wang, C.-Y., Chien, S.-Y., Chen, M.-Z., 2014. A two-way coupled simulation of moving solids in free-surface flows. Computers & Fluids 100, 347–355.

Wu, X., Kofman, J., 2004. Lens distortion calibration by explicit straight-line to distorted-line geometric mapping, in: OpticsEast. International Society for Optics and Photonics, pp. 162–173.

Ye, Z., Mohamadian, H., Ye, Y., 2008. Gray level image processing using contrast enhancement and watershed segmentation with quantitative evaluation, in: ContentBasedMultimediaIndexing,2008.CBMI2008.InternationalWorkshop. IEEE, pp. 470–475.